Computed Tomography Reconstruction from Undersampled Data: An Application to Biomedical Imaging

Zenith Purisha

***Abstract*—In computed tomography, there is often a need to reduce the amount of radiation used due to its potential to alter living tissue properties, especially in the patient or in vivo samples. To achieve this reduction, a method of measuring objects through sparse sampling can be employed. However, in mathematics, this problem leads to an *ill-posed* inverse problem due to limited measurement data. To address this issue, a regularization method is proposed, where the constraint for a regularized solution is enforced by utilizing Daubechies wavelet expansion coefficients. In this work, the algorithm is iteratively computed, employing a soft-thresholding operation for the coefficients, with the thresholding parameter automatically selected. For the purpose of biomedical imaging, we propose incorporating prior knowledge of the thresholding parameter value based on a biological object. The method is tested on simulated data using the chest phantom and real data obtained from the ladybug X-ray measurements.**

***Index Terms*—computed tomography, wavelets, Daubechies, sparsity, regularization, adaptive, under-sampled data, biomedical imaging**

I. Introduction

X-RAY tomography imaging, also known as computed tomography (CT), has found extensive applications in various fields such as medicine and industry. In this imaging techniques, an object is exposed to X-rays from multiple angles, and the resulting data for each angle is recorded [1], [2], [3], [4]. Subsequently, a computer processes the recorded data to generate a reconstructed image, which is the displayed on a screen. The conventional approach to reconstructing the image from complete sets of projections is well understood and considered as a well-established area of research [2].

Unfortunately, in the field of biomedical imaging, the arrangement of the measurement setup often hinders the acquisition of complete sets of projections. This limitation is evident in dental imaging and mammography, where only specific areas of the patient can be exposed to X-rays [5], [6]. Similarly, when dealing with living organisms, excessive exposure to X-ray radiation can be harmful. As a result, the conventional reconstruction technique, which requires complete sets of projections, can no longer be simply called. In mathematics, this problems is *ill-posed*, which means the problem either has *no solution* or has *many solutions*, or the solution procedure is *unstable* [7].

This paper introduces a variational mathematical model for image reconstruction. The primary objective of this proposed approach is to address the *ill-posedness* of the problem by incorporating sparsity constraints on the image using a linear sparsifying transform. Several well-known techniques that employ sparsity-based inversion have been extensively explored in previous studies [8], [9], [10], with applications specifically focused on under-sampled computed tomography investigated in [11], [12]. In this work, we consider orthonormal Daubechies wavelets basis as the sparsifying transform due to its cost-effectiveness and its ability to preserve reconstruction quality [13], [14]. The Daubechies wavelet, known for its vanishing moments property, offers superior performance when applied to natural images [9].

The resulting a functional form is as follows

$$\boldsymbol{f}_{\mathrm{S}} = \underset{\boldsymbol{f}\in\mathbb{R}^{N^2},\, \boldsymbol{f}\geq 0}{\operatorname{argmin}} \left\{ \frac{1}{2}\|\mathbf{A}\boldsymbol{f} - \boldsymbol{y}\|_2^2 + \mu\|\mathbf{W}_D\boldsymbol{f}\|_1 \right\}, \quad (1)$$

where $\boldsymbol{f}$ is the unknown object, $\mathbf{A}$ is tomographic measurement matrix, $\boldsymbol{y}$ is the tomographic measured data, $\mathbf{W}_D$ is Daubechies wavelet matrix and μ as a regularization parameter.

To address the solution of the variational model 1, CWDS algorithm [15], a recently controlled method for regularization parameter is implemented. The algorithm enables to find a thresholding value μ automatically to a desired sparsity level of the sparsifying coefficient. In this work, we propose a desired sparsity that is investigated for biomedical imaging purposes. In many biomedical applications, CT is used to reveal internal organs such as bone, soft tissue, and blood vessel [11], [16]. Computational experiments are performed on both simulated and real data, an insect ladybug, as it supports the motivation in this paper. The real data is measured with a μCT system at the Department of Electrical Engineering, Aalto University (Finland).

Under-sampled CT problem is always receiving attention, however, the use of Daubechies wavelet with automatic choice for thresholding parameter μ for biological tissue image has never been done before. A *prior* information of the desired sparsity level of the thresholding parameter based on biological object is also a new concept. The computation results are compared to the traditional reconstruction method so-called filtered backprojection (FBP) [2].

The paper is organized as follows. In Section II a minimization formulation for the 2D under-sampled CT problem by enforcing sparsifying is introduced. The algorithm to overcome the variational problem is addressed in Section IV. Section V shows the results of the proposed method with a comparison to the FBP approach. Lastly, the discussion and some conclusions are in Section VI and Section VII, respectively.

Manuscript received March 15, 2023; revised November 12, 2023.

Zenith Purisha is an Assistant Professor at the Department of Mathematics, Universitas Gadjah Mada, Indonesia. E-mail: zenith.purisha@ugm.ac.id

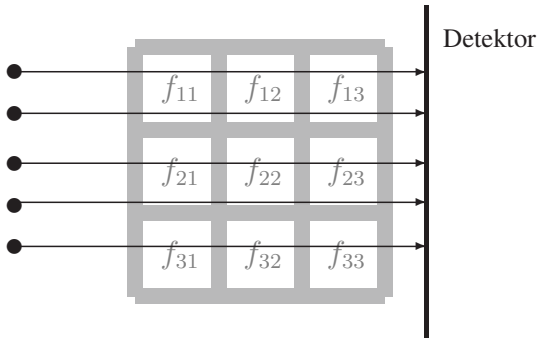

Fig. 1. A representation of X-ray tomographic measurement.

II. Sparsity regularization for under-sampled CT data

In X-ray tomography, the incoming photons of X-ray is recorded in a detector and the X-ray measurement data are put together from the intensity losses of X-rays from different angles of view. In this case, the number of angles of view is sparse. Given an unknown attenuation coefficient function $f(x)$ of the tissue or inner material at the point x. The beam L represents a straight line that carries intensity that passed the object. The X-ray measurement data is modeled by a line integral of $f(x)$. From this integral, we reconstruct the object f.

Let $\Omega \subset \mathbb{R}^2$ as a physical domain and $f : \Omega \subset \mathbb{R}^2 \to \mathbb{R}_+$ as a non-negative attenuation function. In practice, a discrete model is necessary. In two-dimensional, f is represented by a matrix $\boldsymbol{f} = [\tilde{f}_{ij}] \in \mathbb{R}^{N\times N}$. It is represented in Figure 1.

The measurements after calibration can be modeled as follows

$$\int_L f(x)\, ds = \sum_{i=1}^{N}\sum_{j=1}^{N} a_{ij}\tilde{f}_{ij}, \tag{2}$$

and a_{ij} is the length in which the X-ray line L travels through the pixel (i, j).

Tomographic measurement data is then given as:

$$\boldsymbol{y} = \mathbf{A}\boldsymbol{f}, \tag{3}$$

where $\mathbf{A} = [a_{ij}] \in \mathbb{R}^{M\times N^2}$ is the measurement matrix, and $\boldsymbol{y} \in \mathbb{R}^M$ is the measured data.

It is well understood that for under-sampled data, the linear system in 3 leads to highly ill-posed discrete inverse problem. In this case, the solution is not unique (has many solutions). Hence, this problem calls for regularization. Consider a variational functional of the form

$$R(\boldsymbol{f}) = \frac{1}{2}\|\mathbf{A}\boldsymbol{f} - \boldsymbol{y}\|_2^2 + R_1(\boldsymbol{f}). \tag{4}$$

being $R_1(\boldsymbol{f})$ incorporates *a priori* information on the unknown object. We consider ℓ_1-norm of a sparsifying transform. We are interesting in denoising and to this end, Daubechies wavelet is used. Thus, our proposed regularization term has the following form:

$$R_1(\boldsymbol{f}) = \mu\|\mathbf{W}_D\boldsymbol{f}\|_1, \tag{5}$$

where μ is the regularization parameter, $\mathbf{W}_D$ is the matrix of the underlying Daubechies wavelet transform and $\boldsymbol{f}$ is the discrete representation of the unknown object. All together, the proposed constrained minimization problem reads as:

$$\underset{\boldsymbol{f}\in\mathbb{R}^{N^2},\, \boldsymbol{f}\geq 0}{\operatorname{argmin}} \frac{1}{2}\|\mathbf{A}\boldsymbol{f} - \boldsymbol{y}\|_2^2 + \mu\|\mathbf{W}_D\boldsymbol{f}\|_1, \tag{6}$$

where we use the non-negativity solution for $\boldsymbol{f}$. We consider the prior knowledge of $\boldsymbol{f}$ that measures the incoming photon, not strengthening or producing photon.

III. 2D Daubechies wavelets

In this section, we briefly discuss here the main ideas about Daubechies wavelets.

Consider the two real-valued functions $\varphi(x)$ and $\psi(x)$ defined on the interval $[0, 1]$. Generally, $\varphi(x)$ is referred to as a *scaling function* and $\psi(x)$ as a *mother wavelet*. A *discrete Daubechies wavelet system*, where discrete means that the transform is associated with a discrete parameter set, is built by appropriately scaling and translating the mother wavelet $\psi(x)$:

$$\psi_{jk}(x) := 2^{j/2}\psi(2^j x - k) \qquad \text{for } j \leq 0,\ 0 \leq k \leq 2^j - 1,$$

and the scaling function $\varphi(x)$:

$$\varphi_{jk}(x) := 2^{j/2}\varphi(2^j x - k) \qquad \text{for } j \leq 0,\ 0 \leq k \leq 2^j - 1,$$

where $\varphi(x) = 0$ for $x < 0$ and $x > 1$. Here, $j,\ k \in \mathbb{Z}$. The shape of the mother wavelet and scaling function are shown in Figure 2 and Figure 3.

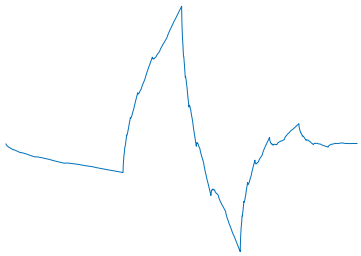

Fig. 2. Mother wavelet

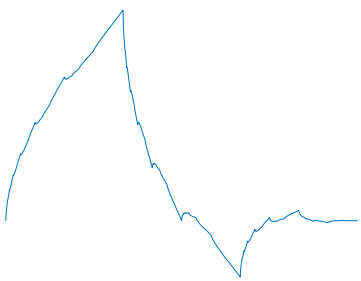

Fig. 3. Scaling function

It is well known that the above 1D construction leads to an orthonormal system. In 2D, we consider the standard tensor-product extension of the 1D Daubechies wavelet transform. In detail, a 2D Daubechies system is spanned by four types of functions. Three of these types have the following form:

$$\varphi_{jk}(x)\psi_{jk}(y), \quad \psi_{jk}(x)\varphi_{jk}(y), \quad \psi_{jk}(x)\psi_{jk}(y), \tag{7}$$

and the fourth type is given by $\varphi_{j_0k}(x)\varphi_{j_0k}(y)$. Notice that the fourth type describes the coarsest scale j_0. The associated matrix underlying the *discrete wavelet transform* of a function $\boldsymbol{f}$ is given by

$$\mathbf{W}_D = \begin{bmatrix} W_\varphi & W_\psi^V \\ W_\psi^H & W_\psi^D \end{bmatrix} \in \mathbb{R}^{N^2 \times N^2}$$

where

$$W_\varphi = \frac{1}{\sqrt{RS}} \sum_{r=1}^{R} \sum_{s=1}^{S} \boldsymbol{f}\{q\}\, \varphi_{j_0k}\{r\}\varphi_{j_0k}\{s\} \tag{8}$$

$$W_\psi^H = \frac{1}{\sqrt{RS}} \sum_{r=1}^{R} \sum_{s=1}^{S} \boldsymbol{f}\{q\}\, \psi_{jk}\{r\}\varphi_{jk}\{s\} \tag{9}$$

$$W_\psi^V = \frac{1}{\sqrt{RS}} \sum_{r=1}^{R} \sum_{s=1}^{S} \boldsymbol{f}\{q\}\, \varphi_{jk}\{r\}\psi_{jk}\{s\} \tag{10}$$

$$W_\psi^D = \frac{1}{\sqrt{RS}} \sum_{r=1}^{R} \sum_{s=1}^{S} \boldsymbol{f}\{q\}\, \psi_{jk}\{r\}\psi_{jk}\{s\} \tag{11}$$

being $q = r + R*(s-1)$, and the brackets $\{\cdot\}$ indicate that we now intend also ϕ and ψ as discrete functions defined in the intervals $[1, R]$ or $[1, S]$, being $R,\, S \in \mathbb{Z}$.

Thus, the vector collecting all the wavelet coefficients is given by:

$$\mathbf{W}_D \boldsymbol{f} \ \in \mathbb{R}^{N^2}. \tag{12}$$

With the above notation, the minimization problem (4) reads as

$$\boldsymbol{f}_{\mathrm{S}} = \underset{\boldsymbol{f} \in \mathbb{R}_+^{N^2}}{\operatorname{argmin}} \left\{ \frac{1}{2}\|\mathbf{A}\boldsymbol{f} - \boldsymbol{y}\|_2^2 + \mu \|\mathbf{W}_D \boldsymbol{f}\|_1 \right\}. \tag{13}$$

One of the main benefit of wavelets is that the transform coefficients are easy to compute and many fast algorithmic implementation are available.

For more information about the Daubechies wavelet transform, and its implementation, we refer to the classic text [14].

IV. Adaptive Iterative Thresholding Algorithm

A. Controlled Wavelet Domain Sparsity Algorithm

We use a recently algorithm Controlled Wavelet Domain Sparsity (CWDS) algorithm for the solution of the optimization problem 1 as studied in [15] by exploiting different basis. A step-by-step algorithm is outlined in Algorithm 1. It is a primal-dual method [17] in which the regularization parameter μ is determined automatically using a control algorithm driving the sparsity of the image reconstruction to an *a priori* known level of sparsity. The minimizer of (1) can be computed as:

$$\begin{aligned} \boldsymbol{y}_{(i+1)} &= \mathbb{P}_C\Big(\boldsymbol{f}_{(i)} - \tau \nabla g(\boldsymbol{f}_{(i)}) - \lambda \mathbf{W}_D^T \boldsymbol{v}_{(i)}\Big) \\ \boldsymbol{v}_{(i+1)} &= \Big(I - \mathcal{T}_\mu\Big)\Big(\mathbf{W}_D \boldsymbol{y}_{(i+1)} + \boldsymbol{v}_{(i)}\Big) \\ \boldsymbol{f}_{(i+1)} &= \mathbb{P}_C\Big(\boldsymbol{f}_{(i)} - \tau \nabla g(\boldsymbol{f}_{(i)}) - \lambda \mathbf{W}_D^T \boldsymbol{v}_{(i+1)}\Big) \end{aligned} \tag{14}$$

where τ and λ are positive parameters, $g(\boldsymbol{f}) = \frac{1}{2}\|\mathbf{A}\boldsymbol{f} - \boldsymbol{y}\|_2^2$, and $\mathcal{T}$ is a soft-thresholding operator and reads as

$$\mathcal{T}_\mu(c) = \begin{cases} c + \frac{\mu}{2} & \text{if } \ c \le -\frac{\mu}{2} \\ 0 & \text{if } \ |c| < \frac{\mu}{2} \\ c - \frac{\mu}{2} & \text{if } \ c \ge -\frac{\mu}{2}. \end{cases} \tag{15}$$

Regularization parameter $\mu > 0$ represents the thresholding parameter. Parameters τ and λ are parameters which guarantee convergence. In detail, $0 < \lambda < 1/\lambda_{\max}(\mathbf{W}_D \mathbf{W}_D^T)$, where $\lambda_{\max}$ is the maximum eigenvalue, here $0 < \tau < 2/\tau_{\text{lip}}$, and τ_{lip} is the Lipschitz constant for $g(\boldsymbol{f})$. Notation $C = \mathbb{R}_+^{N^2}$ represents the non-negative quadrant and $\mathbb{P}_C$ is the Euclidian projection.

B. Adaptive thresholding parameter μ

The idea using proportional-integral-derivative (PID) controllers [18], [19], [20] is considered to change parameter μ adaptively. Some recent applications may be found in [21], [22]. Assume that if C_{pr} is the known degree of sparsity and C_i is the degree of sparsity at i^{th} iteration, then the μ changes as follows:

$$\mu_{(i+1)} = \mu_{(i)} + \beta(C_{(i)} - C_{pr}),$$

where β is tuning parameter of the controller. The value of β is determined based on Daubechies wavelet coefficients of the backprojection reconstruction of the object.

In this work, we define C_{pr} differrently as it is done in [15]. We assume that we have available an object (or objects) $\boldsymbol{f}_{pr}$ which can be similar to the one we are imaging. In this case, $\boldsymbol{f}_{pr}$ is the FBP reconstruction image of an axial slice of the insect using a full angle of data.

For a vector $w \in \mathbb{R}^{N^2}$ we define the number of elements larger than ν:

$$\#_\nu w := \#\{\, i \ | 1 \le i \le N^2, \ |w_i| > \nu\}.$$

Now, the prior sparsity level is defined by

$$C_{pr} = \frac{\#_\nu\{\mathbf{W}_D \boldsymbol{f}_{pr}\}}{N^2}, \tag{16}$$

where N^2 is the total number of coefficients and $\mathcal{C}_{C_{pr}}$ is the largest C_{pr} Daubechies wavelet coefficients of $\boldsymbol{f}_{pr}$.

The prior sparsity level C_{pr} is chosen when ν gives $\|\boldsymbol{f}_{pr} - IWT(\mathcal{C}_{C_{pr}})\| < \epsilon$, where IWT is an inverse Daubechies wavelet transform where the value of ϵ is set to be very small but positive.

V. Numerical Experiments

In this Section, numerical results are shown for undersampled data of simulated data (see section V-B) and real data (see section V-C). The reconstructions are computed using 30 and 15 directions. All the algorithms were implemented in Matlab 9.11 (R2021b) and performed on Apple M1 and CPU 8GB memory. The Daubechies wavelet matrix $\mathbf{W}_D$ is generated by using Spot–A Linear-Operator Toolbox [23]. The number of scales for the wavelet transform is set equal to 2. In all experiments, parameters ϵ_1 and ϵ_2 that control the stopping criterion have been set equal to 10^{-2}. We also set parameters $\beta = 10^{-3}$ and $\mu_{(0)} = 10^{-4}$. The prior sparsity level computed using 16 is 60%.

Algorithm 1 An Automatic Iterative Thresholding Algorithm using Daubechies Wavelet

Inputs: measurement data vector $\boldsymbol{y}$, system matrix $\mathbf{A}$, parameters τ, $\lambda > 0$ to ensure convergence, *a priori* degree of sparsity C_{pr}, initial thresholding parameter $\mu_{(0)}$, maximum number of iterations $I_{\max} > 0$, parameter tolerances $\epsilon_1, \epsilon_2 > 0$ for the stopping rule, and control stepsize $\beta > 0$.
$\boldsymbol{f}_{(0)} = \mathbf{0}$, $i = 0$, $e = 1$, and $C_{(0)} = 1$
while $i < I_{\max}$ and $|e| \geq \epsilon_1$ or $d \geq \epsilon_2$ **do**
  $e = C_{(i)} - C_{pr}$
  if $\operatorname{sign}(e_{(i+1)}) \neq \operatorname{sign}(e_{(i)})$ **then**
    $\beta = \beta(1 - |e_{(i+1)} - e_{(i)}|)$
  $\mu_{(i+1)} = \max\{0, \mu_{(i)} + \beta e\}$
  $\boldsymbol{y}_{(i+1)} = \max\{0, \boldsymbol{f}_{(i)} - \gamma \nabla g(\boldsymbol{f}_{(i)}) - \lambda \mathbf{W}_D^T \boldsymbol{v}_{(i)}\}$
  $\boldsymbol{v}_{(i+1)} = (I - \mathcal{T}_{\mu_{(i)}})(\mathbf{W}_D \boldsymbol{y}_{(i+1)} + \boldsymbol{v}_{(i)})$
  $\boldsymbol{f}_{(i+1)} = \max\{0, \boldsymbol{f}_{(i)} - \gamma \nabla g(\boldsymbol{f}_{(i)}) - \lambda \mathbf{W}_D^T \boldsymbol{v}_{(i+1)}\}$
  $C_{(i+1)} = N^{-2} \#_\nu(\mathbf{W}_D \boldsymbol{f}_{(i+1)})$
  $d = \|\boldsymbol{f}_{(i+1)} - \boldsymbol{f}_{(i)}\|_2 / \|\boldsymbol{f}_{(i+1)}\|_2$
  $i := i + 1$

A. Acquisition data

Our proposed approach is tested on simulated data (see Section V-B) and real data (see Section V-C) test the algorithm using 30 and 15 directions uniformly sampled out of 360 degrees.

B. Simulated data: chest phantom

We use the chest phantom generated with Matlab (see Figure 4). The phantom is sized $N \times N$, with $N = 128$. The projection data (*i.e.*, sinogram) of the simulated phantom is corrupted by a white Gaussian noise with zero mean and 0.1% variance. The phantom will be used as a ground truth of the experiment.

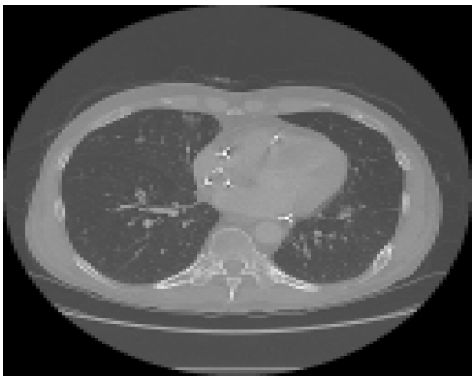

Fig. 4. The chest phantom generated with Matlab. The phantom is used as a ground truth.

C. Real data: an insect

We use the tomographic X-ray real data of a ladybug (see Figure 5), consisting of a 2D cross-section of a ladybug measured with CT device available at Aalto University (Finland). The dataset is available and freely downloadable at here. For a detailed documentation of the acquiring setup, including the specifications of the X-ray systems, see [24].

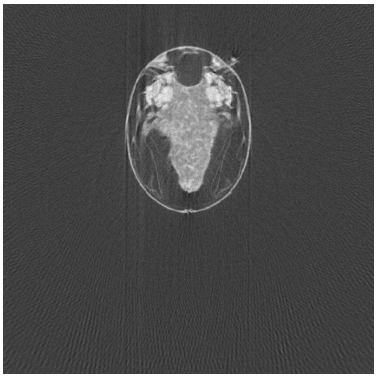

Fig. 5. Full-data-reconstructed axial slice of ladybug using FBP.

D. Numerical results

In this section, the results of the experiments using the proposed method are reported. Figure 7 and Figure 6 presents the reconstruction images of the chest phantom using tomographic data addressed in Section V-B. In the columns, left and right, we collect results from traditional reconstruction, filtered backprojection (FBP), and the proposed method. Table I shows the figure of merits for chest phantom reconstruction. We report the relative error, peak-signal-to-noise ratio (PSNR), and the structural similarity index (SSIM) in Table I.

The image reconstructions of the insect (ladybug) are shown in Figure 8 for 30 directions and Figure 9 for 15 directions. As in real data, the ground truth is not as at our disposal, figures of merit are not available. We do, however, present FBP reconstructions from complete and dense projections for qualitative analysis. The reconstructions of the insect using FBP and the proposed approach are shown on the left image (a) and the right image (b), respectively.

The proposed method, as discussed in Section IV-B, implements a controlled wavelet domain sparsity (Algorithm 1). The matrix A is the measurement matrix generated in 2. The measurement data vector $\boldsymbol{y}$ is obtained from V-B and V-C . The parameters τ and λ are chosen to be 1 and 0.99, respectively.

Figure 10 shows the plot of the sparsity levels as the iteration progresses. The stopping rule is satisfied when the error between the degree of sparsity and the *a priori* degree of sparsity is less than $\epsilon_1 = 10^{-2}$. The sparsity level increases initially and then rapidly decreases toward the a priori degree of sparsity level. This confirms that the sparsity level converges to the desired sparsity after 60 iterations for 30 projections data and 100 iterations for 15 projections data.

The computation time are reported in Table II and Table III. It is shown that the proposed approach require long computation time compared to FBP method.

VI. Discussion

In this paper, we propose a novel approach for reconstructing CT images from under-sampled measurement data

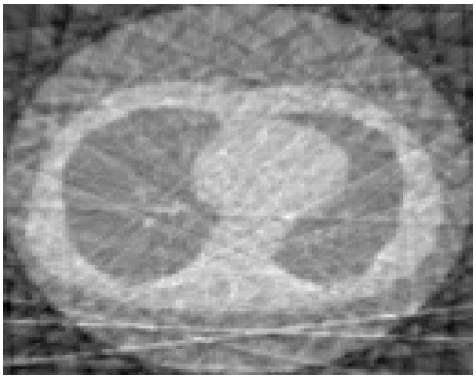

(a)

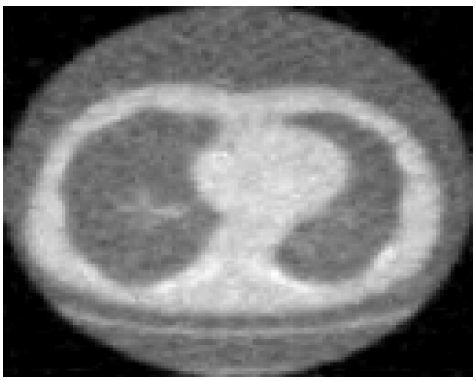

(b)

Fig. 6. (a) The FBP reconstruction of the chest phantom using 30 projections. (b) The proposed approach reconstruction of the chest phantom using 30 projections.

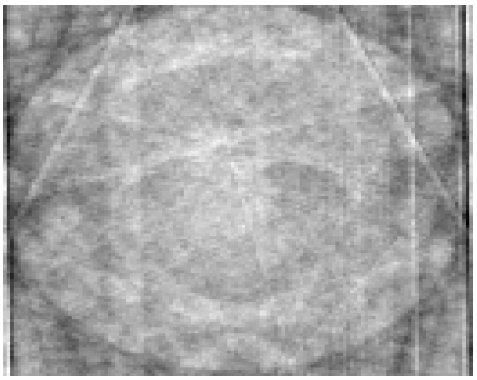

(a)

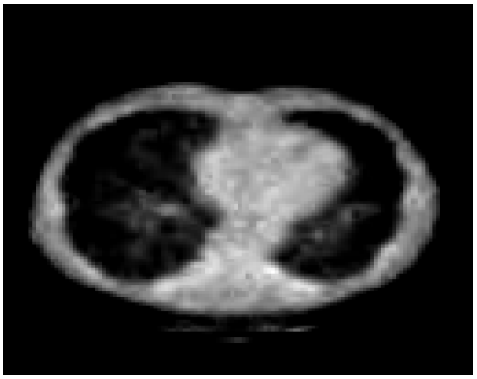

(b)

Fig. 7. (a) The FBP reconstruction of the chest phantom using 15 projections. (b) The proposed approach reconstruction of the chest phantom using 15 projections.

TABLE I
FIGURES OF MERIT FOR THE CHEST PHANTOM RECONSTRUCTIONS USING FBP AND PROPOSED APPROACH WITH 30 PROJECTIONS.

Methods	Relative Error	PSNR	SSIM
FBP	0.08	22.12	0.46
Proposed approach	0.04	27.31	0.72

TABLE II
COMPUTATION TIME (IN SECONDS) FOR THE CHEST PHANTOM RECONSTRUCTIONS USING FBP AND PROPOSED APPROACH WITH 30 AND 15 PROJECTIONS.

Methods	30 projections	15 projections
FBP	0.12	0.08
Proposed approach	81	202

TABLE III
COMPUTATION TIME (IN SECONDS) FOR THE LADYBUG RECONSTRUCTIONS USING FBP AND PROPOSED APPROACH WITH 30 AND 15 PROJECTIONS.

Methods	30 projections	15 projections
FBP	1.4	0.17
Proposed approach	64	96

using an adaptive wavelet domain sparsity algorithm. The Daubechies wavelet is implemented. Our proposed approach is evaluated on simulated chest data as described in V-B and real data, an axial slice of an insect, a ladybug, which contains biological tissue, as described in V-C, using only 15 and 30 projection views. The mathematical model is formulated as a minimization constraint with a linear sparsifying wavelet transform in the penalty term. Among many kinds of wavelets, Daubechies wavelet transform is chosen. To address the solution, the thresholding parameter that appears in the regularization term is set adaptively.

For 30 projections of X-ray tomographic data, the proposed technique reduces the relative error of the chest phantom reconstruction to half that of the FBP reconstruction. The PSNR of the proposed approach is 27.31. It is higher than PSNR in the FBP reconstruction, 22.12. The higher the PSNR, the better is the quality of the image. The relative error of the proposed approach is 0.04, half that of the FBP reconstruction. In the proposed approach, the SSIM is reported 0.72, and the FBP reconstruction has lower value of SSIM, 0.46. Overall, quantitatively, the reconstruction of the proposed approach, the adaptive wavelet domain sparsity algorithm, shows better results quality in terms of image quality metrics. The result demonstrates that the reconstruction of simulated data using the proposed method outperforms FBP reconstructions in terms of relative error, PSNR, and SSIM.

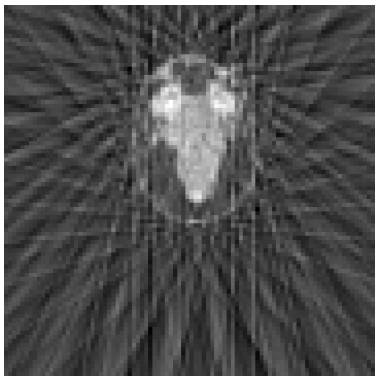

(a)

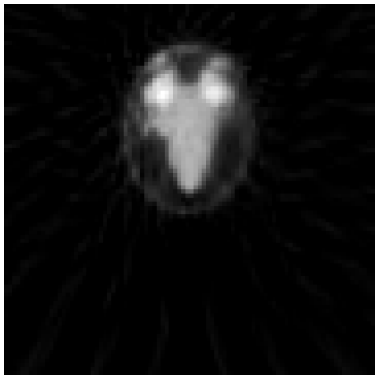

(b)

Fig. 8. (a) FBP reconstructions of an axial slice of ladybug using 30 projection. (b) Proposed approach reconstruction of an axial slice of ladybug using 30 projections.

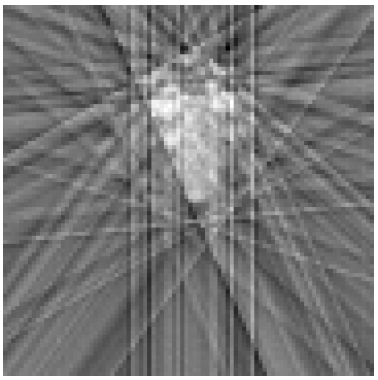

(a)

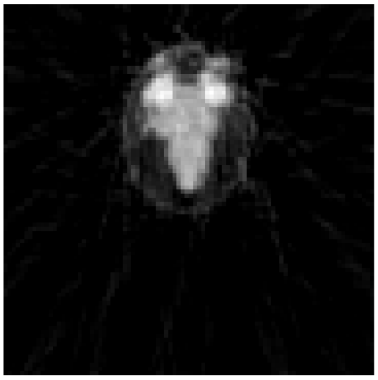

(b)

Fig. 9. (a) FBP reconstructions of an axial slice of ladybug using 15 projection. (b) Proposed approach reconstruction of an axial slice of ladybug using 15 projections.

The FBP reconstruction of the chest phantom using 15 projections yields only artifacts almost in all regions. Using the proposed method, the chest reconstruction from 15 projection data recovers the singularity well, including the edges inside and outside the object. The reconstruction image is not dominated by artifacts.

In the FBP reconstruction, the image is dominated by artifacts. It is also evident that, because a non-negativity constraint is not available in the FBP algorithm, pixels with zero or extremely low attenuated values are poorly represented. As we can see from the results of the proposed approach, the artifacts are considerably less visible. A deeper examination reveals that the non-negativity constraint enhances the reconstructions. It is noticeable in the FBP reconstruction that the thin long line on the bottom area of the chest is covered by line artifacts, mostly to the angular sub-sampling, whilst with the proposed approach the thin line has recovered with visible edges.

In real data reconstruction, the FBP reconstruction is more dominated by artifacts than the proposed-approach reconstruction. In particular, the reconstructions produced by the proposed approach yield finer features in the image with fewer artifacts. The image quality is also improved since the background of the image and certain interior regions of the object that correspond to zero-attenuation coefficients were projected to zero values using the non-negativity penalty. Dominant features of the ladybug, such as the axial slicing of the eyes and the body, are also well recovered.

Despite its success, the computational burden of the proposed method is high (up to 81 and 202 seconds), as it can be seen in Table II and Table III. However, the computation time could be sped-up by implementing paralellized GPU code.

VII. Conclusion

This paper presents a novel approach for reconstructing CT images from under-sampled data. The method incorporates adaptive tuning on the regularization parameter through the use of a sparsity-promoting penalty, employing an orthonormal wavelet basis known as Daubechies. Comparative evaluations demonstrate that the reconstructed images from simulated data obtained using the proposed method exhibit superior image quality compared to the conventional FBP algorithm. The evaluation metrics used to assess image quality include relative error, PSNR, and SSIM.

The algorithm is tested as well on real tomographic data of an insect. The optimal values for sparsity and thresholding parameters could be utilized to reconstruct X-ray tomographic data from various biological tissues. Nonetheless, it is worth noting that the same algorithm and procedures can be applied to various other tomographic applications.

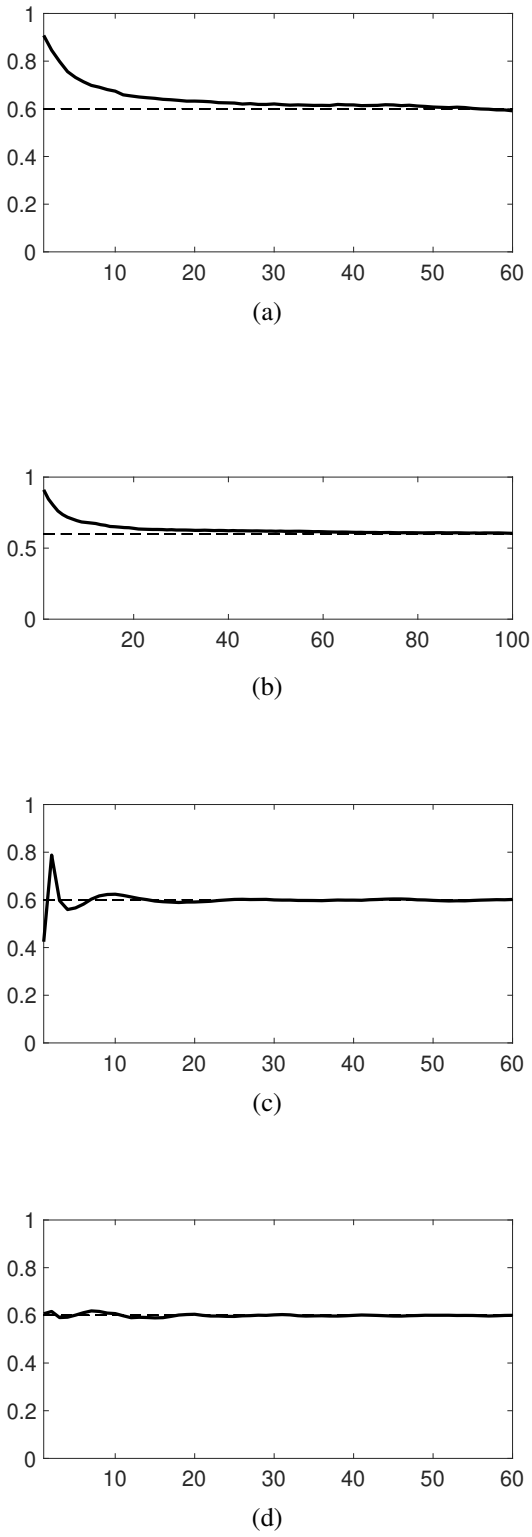

Fig. 10. The ratio of nonzero Daubechies wavelet coefficients as the iteration progresses for the chest phantom data using 30 and 15 projections data ((a) and (b)). The ratio of nonzero Daubechies wavelet coefficients as the iteration progresses for the ladybug data using 30 and 15 projection data ((c) and (d)).

REFERENCES

[1] A. C. Kak and M. Slaney, *Principles of computerized tomographic imaging*. SIAM, 2001.

[2] F. Natterer and F. Wübbeling, *Mathematical methods in image reconstruction*. SIAM, 2001.

[3] L. A. Shepp and J. Kruskal, "Computerized tomography: the new medical x-ray technology," *American Mathematical Monthly*, vol. 85, no. 6, pp. 420–439, 1978.

[4] S. P. Sugandha Saxena and D. M. T. S, "Utilizing deep learning techniques to diagnose nodules in lung computed tomography (ct) scan images," *IAENG International Journal of Computer Science*, vol. 50, no. 2, pp. 537–552, 2023.

[5] M. Rantala, S. Vanska, S. Jarvenpaa, M. Kalke, M. Lassas, J. Moberg, and S. Siltanen, "Wavelet-based reconstruction for limited-angle x-ray tomography," *IEEE transactions on medical imaging*, vol. 25, no. 2, pp. 210–217, 2006.

[6] K. Hämäläinen, A. Kallonen, V. Kolehmainen, M. Lassas, K. Niinimäki, and S. Siltanen, "Sparse tomography," *SIAM Journal on Scientific Computing*, vol. 35, no. 3, pp. B644–B665, 2013.

[7] J. L. Mueller and S. Siltanen, *Linear and nonlinear inverse problems with practical applications*. SIAM, 2012.

[8] P.-L. Lions and B. Mercier, "Splitting algorithms for the sum of two nonlinear operators," *SIAM Journal on Numerical Analysis*, vol. 16, no. 6, pp. 964–979, 1979.

[9] I. Daubechies, M. Defrise, and C. De Mol, "An iterative thresholding algorithm for linear inverse problems with a sparsity constraint," *Communications on pure and applied mathematics*, vol. 57, no. 11, pp. 1413–1457, 2004.

[10] I. Loris and C. Verhoeven, "On a generalization of the iterative soft-thresholding algorithm for the case of non-separable penalty," *Inverse Problems*, vol. 27, no. 12, p. 125007, 2011.

[11] Z. Purisha, S. S. Karhula, J. H. Ketola, J. Rimpeläinen, M. T. Nieminen, S. Saarakkala, H. Kröger, and S. Siltanen, "An automatic regularization method: An application for 3-d x-ray micro-ct reconstruction using sparse data," *IEEE transactions on medical imaging*, vol. 38, no. 2, pp. 417–425, 2018.

[12] T. A. Bubba, D. Labate, G. Zanghirati, and S. Bonettini, "Shearlet-based regularized reconstruction in region-of-interest computed tomography," *Mathematical modelling of natural phenomena*, vol. 13, no. 4, p. 34, 2018.

[13] S. Mallat, *A wavelet tour of signal processing*. Elsevier, 1999.

[14] I. Daubechies, *Ten lectures on wavelets*. SIAM, 1992.

[15] Z. Purisha, J. Rimpeläinen, T. Bubba, and S. Siltanen, "Controlled wavelet domain sparsity for x-ray tomography," *Measurement Science and Technology*, vol. 29, no. 1, p. 014002, 2017.

[16] A. Webb, *Introduction to biomedical imaging*. John Wiley & Sons, 2022.

[17] P. Chen, J. Huang, and X. Zhang, "A primal-dual fixed point algorithm for minimization of the sum of three convex separable functions," *Fixed Point Theory and Applications*, vol. 2016, no. 1, p. 54, 2016.

[18] K. J. Åström and T. Hägglund, *PID controllers: theory, design, and tuning*. ISA Research Triangle Park, NC, 1995.

[19] M. Araki, "Pid control," *Control Systems, Robotics and Automation: System Analysis and Control: Classical Approaches II, Unbehauen, H.(Ed.). EOLSS Publishers Co. Ltd., Oxford, UK., ISBN-13: 9781848265912*, pp. 58–79, 2009.

[20] S. Bennett, *A history of control engineering, 1930-1955*. IET, 1993, no. 47.

[21] M. Bueno-Lopez and E. Giraldo, "Real-time pid adaptive decoupled controller applied over a dc-dc multivariable boost converter." *Engineering Letters*, vol. 30, no. 4, pp. 1551–1557, 2022.

[22] K. Kankhunthodl, V. Kongratana, A. Numsomran, and V. Tipsuwanporn, "Self-balancing robot control using fractional-order pid controller," in *Lecture Notes in Engineering and Computer Science: Proceedings of The International MultiConference of Engineers and Computer Scientists*, 2019, pp. 13–15.

[23] E. Van den Berg and M. Friedlander, "Spot – a linear-operator toolbox," http://www.cs.ubc.ca/labs/scl/spot/, accessed: 2013-02-08.

[24] J. Juurakko, Z. Purisha, and S. Särkkä, "Dynamic 3d tomographic x-ray data of ladybug," 2019. [Online]. Available: https://arxiv.org/abs/1908.08782

Zenith Purisha received the M.Sc. degree in mathematics from Department of Mathematics, Universitas Gadjah Mada, Indonesia, in 2011 and the Ph.D. degree in mathematics from Department of Mathematics and Statistics, the University of Helsinki, Finland, in 2018. She did a postdoctoral research at Department of Electrical Engineering and Automation, Aalto University, Finland in 2018 – 2020.

She is currently a lecturer in Department of Mathematics, Universitas Gadjah Mada, Indonesia. Her research interest focuses on developing algorithms for X-ray tomography application from incomplete measurement data.